Contents lists available at ScienceDirect

Applied Catalysis B: Environmental

journal homepage: www.elsevier.com/locate/apcatb

Unpredictable photocatalytic ability of H$_2$-reduced rutile-TiO$_2$ xerogel in the degradation of dye-pollutants under UV and visible light irradiation

Carlos A. Páez [a,*], Dirk Poelman [b], Jean-Paul Pirard [a], Benoît Heinrichs [a]

[a] *Université de Liège, Laboratoire de Génie chimique – Génie catalytique, B6a, B-4000 Liège, Belgium*
[b] *Ghent University, Lumilab, Department of Solid State Sciences, Krijgslaan 281-S1, B-9000 Ghent, Belgium*

ARTICLE INFO

ABSTRACT

A series of H$_2$-reduced TiO$_2$ xerogels of low specific surface area was prepared by the sol–gel process. The gels were dried, calcined in air at various temperatures (400, 500, 700 °C) and then reduced at 400 °C under hydrogen flow (H$_2$-HTR treatment). The materials were characterized by X-ray diffraction, transmission electron microscopy (TEM) and UV/Visible diffuse reflectance spectroscopy, and their texture was determined by nitrogen adsorption–desorption. IR spectroscopy was used to study to what extent samples were reduced. The effects of the calcination/H$_2$-HTR treatments on the adsorption of methylene blue (MB) in aqueous solution and on the photocatalytic degradation of MB and crystal violet (CV) under UV and visible light irradiation were also evaluated. Results showed predictable modifications in the physicochemical properties caused by the annealing of TiO$_2$ xerogel at high temperature (700 °C), such as a total anatase-to-rutile phase transition and a considerable loss of specific surface area from 260 to 2 m^2 g^{-1}. However, the higher degree of reduction exhibited by the rutile-TiO$_2$ lattice led to unpredictable photocatalytic activity for the dye conversion under UV and visible light irradiation. The loss of specific surface area of the rutile-TiO$_2$ sample was compensated by the increase in the affinity of this sample for the dye. Under UV light, the rutile-TiO$_2$ xerogel obtained at 700 °C showed a similar level of photoactivity as the one obtained with anatase-TiO$_2$ xerogels obtained by calcination at 400 and 500 °C. On the other hand, under visible light, unlike anatase-TiO$_2$ xerogels, the rutile-TiO$_2$ xerogel showed a dye photoconversion rate per external surface area that was up to 40 times higher than the one obtained with commercial Degussa P25 TiO$_2$.

© 2009 Elsevier B.V. All rights reserved.

1. Introduction

Photocatalytic degradation of organic and inorganic pollutants on the TiO$_2$ semiconductor has been extensively studied as a way to solve environmental problems relating to wastewater and polluted air [1–3]. Anatase and rutile are the most commonly used crystalline structures of TiO$_2$, with anatase showing a higher photocatalytic activity [4]. Anatase higher activity is usually attributed to its higher specific surface area and its favourable band-gap energy (E_g). However, its high band-gap ($E_g \cong 3.2$ eV) implies the use of UV light ($\lambda \leq 380$ nm) to inject electrons into the conduction band (TiO$_2$(e$^-$$_{CB}$)) and to leave holes in the valence band (TiO$_2$(h$^+$$_{VB}$)) [5]. Thus, in practice, this limits the use of sunlight or visible light as an irradiation source in photocatalytic reactions on anatase-TiO$_2$. Numerous studies have recently been performed to enhance electron–hole separation and to extend the light absorption of TiO$_2$ towards the visible range. These studies include doping with metal ions of the TiO$_2$ lattice [6], dye photosensitization on the TiO$_2$ surface [2,7–9], deposition of noble metals [4,10–13], structural modification by mixing with other metal oxides [13–17], and synthesis of nanocrystalline TiO$_2$ with a lower band gap [18–20].

Although the low band-gap energy of rutile-TiO$_2$ ($E_g \cong 3.02$ eV) allows rutile to potentially absorb more solar energy than anatase [21], the anatase-to-rutile phase transition leads to the collapse of the TiO$_2$ specific surface area [22,23], which may result in a decrease in the photocatalytic activity of rutile [24–28]. Low specific surface area and therefore poor absorption properties lead to strong limitations in exploring the photo-efficiency of rutile. However, rutile-TiO$_2$ has some advantages over anatase-TiO$_2$ such as a higher refractive index, a higher dielectric constant, higher electric resistance and higher chemical stability [29]. Furthermore, rutile has been proved to be comparable to anatase in its photoelectrochemical properties when used in dye-sensitized solar cells [30]. Recently, Zhang et al. [31] synthesized single-phase rutile-TiO$_2$ with high photocatalytic activity for the degradation of rhodamine B under UV irradiation. Mohamed et al. [32] obtained a good activity in the

---

* Corresponding author. Tel.: +32 4 3663541; fax: +32 4 3663545.
E-mail address: cpaez@ulg.ac.be (C.A. Páez).

photocatalytic degradation of methylene blue (MB) dye under visible light irradiation with rutile, by modification of its surface with NH_4VO_3 and $(NH_4)_2SO_4$. They emphasize that the MB degradation can be obtained due to basic sites detected on the modified surface. Those sites can favour the reductive activation of O_2 into superoxides ($O_2^{\bullet-}$) with the photo-induced conduction band electrons ($TiO_2(e^-_{CB})$) [33]. It has been suggested that oxygen and its reduced species ($O_2^{\bullet-}$) play an important role in TiO_2 catalysed photo-mineralization [4]. This oxygen activation requires the presence of TiO_2 surface defect sites, specifically surface oxygen vacancies (such as Ti^{3+}) [34]. Thus, the increase in such defect sites could improve the photo-efficiency on TiO_2 materials with a low specific surface area. In accordance with Yates et al. [4], various coordinatively unsaturated Ti cations (Ti^{3+}, Ti^{2+}, Ti^+) can be generated on TiO_2 surfaces by vacuum annealing, Ar^+ sputtering, or chemical reduction using H_2 or CO_2 flows [34–37]. These defect sites, which appear on the TiO_2 surface, exhibit not only the acid–base properties of most metal oxides, but also oxidation–reduction reactivities.

In the present study, a series of H_2-reduced TiO_2 xerogels of low specific surface area was prepared by sol–gel process, i.e. by hydrolysis and condensation of tetraisopropoxy titanium(IV) in 2-methoxyethanol. The gels were dried, calcined in air at increasing temperatures and finally reduced in H_2 at 400 °C. The effect of the calcination temperature on the crystalline phase, on the final reduction degree of the crystalline lattice, on the adsorption of methylene blue (MB) in solution and on the photocatalytic activity under UV and visible light was evaluated.

2. Experimental

2.1. Synthesis

Tetraisopropoxy titanium(IV) (TIPT, 77.34 mL, 98% Janssen Chemical) was mixed with 206.1 mL of 2-methoxyethanol (Sigma–Aldrich, 99.8%) under a nitrogen atmosphere. The mixture was stirred for 20 min. A solution containing 10.35 mL of distilled water in 206.1 mL of 2-methoxyethanol was then added dropwise to the mixture. The solution vessel was then tightly closed and heated up to 70 °C for 24 h (gelation and ageing). The sample vessel was opened and placed in a drying oven at 70 °C. The pressure was slowly decreased for 72 h down to 1200 Pa and, at that pressure, the temperature was increased up to 150 °C for 24 h. The resulting xerogel was crushed and washed with deionized water and methanol. This sample before heat treatment is referred as Ti-NC.

2.2. Calcination and reduction

Ti-NC was calcined at three different temperatures: 400, 500 and 700 °C. The sample was heated at a rate of 120 °C h^{-1} under flowing air (0.1 mmol s^{-1}) and the temperature was maintained for 12 h. After calcination, the samples were reduced by heating them, in pure flowing hydrogen (0.23 mmol s^{-1}) at a rate of 400 °C h^{-1} up to 400 °C and that temperature was maintained for 3 h (H_2-high temperature reduction, H_2-HTR). The calcined and reduced samples are referred as Ti-400, Ti-500 and Ti-700. Commercially available TiO_2 (Degussa P25) was used as a reference photocatalyst. It is referred to as P25.

2.3. Characterization

The crystalline structure of all samples was determined by XRD with a Siemens D5000 X-ray diffractometer using the Cu-Kα radiation. The mean crystallite size were estimated by transmission electron microscopy (TEM, JEOL JEM-4000EX) operated at an accelerating voltage of 400 kV. The texture of the xerogels was examined by nitrogen adsorption–desorption. Isotherms were measured at 77 K with a Fisons Sorptomatic 1990 after outgassing at 10^{-3} Pa for 24 h at ambient temperature. Those isotherms provide the BET specific surface area, S_{BET}, and the pore volume calculated from the adsorbed volume at saturation, V_p [13,38].

Diffuse reflectance measurements in the UV/vis region (250–800 nm) (DR-UV/Vis) were performed on a Varian Cary 5000 UV/Vis/NIR spectrophotometer, equipped with a Varian External DRA-2500 integrating sphere, using $BaSO_4$ as the reference. UV/vis spectra were recorded in diffuse reflectance mode (R = reflection intensity) and were transformed into the absorbance coefficient ($F(R)$) by the Kubelka–Munk function, $F(R) = (1 - R)^2/2R$ [39]. For the sake of comparison, all spectra were arbitrarily normalized in intensity to 1.0. Band-gap values, E_g, were obtained from the plot of the Kubelka–Munk function $(F(R)E)^{1/2}$ vs. the energy of the absorbed light, E [13,40].

FT-IR spectra of all samples were recorded with a Bruker IS-88 spectrometer at room temperature in the region of 400–4000 cm^{-1} (resolution 4 cm^{-1}; 16 scans/spectrum). Xerogel powders were dispersed in KBr by mixing 5 mg of TiO_2 powder with 0.495 g of KBr, and by hydraulically pressing the mixture into the shape of a disc.

2.4. Adsorption isotherms of methylene blue (MB)

All batch equilibrium experiments were conducted in the dark at 30 °C for 24 h. 5 mg of TiO_2 powder was suspended in 5 mL of MB ($C_{16}H_{18}N_3ClS$) solutions at various concentrations (from 0.16 to 7.5 µmol L^{-1}). The equilibrium concentration was determined by UV/Vis spectroscopy (Schimadzu UV-3101 at 664 nm) after centrifugation and filtration of the suspensions. Analyses of the adsorption isotherms of MB were performed by applying the linear Langmuir model equation:

$$\frac{1}{\eta} = \frac{1}{\eta_{max}K_L} \times \frac{1}{C_{eq}} + \frac{1}{\eta_{max}} \tag{1}$$

where C_{eq} and η are the amounts of MB in solution (µmol L^{-1}) and on the solid (µmol g^{-1}), respectively. η_{max} is the amount of adsorbate at monolayer coverage (µmol g^{-1}) and K_L is the Langmuir equilibrium constant (L µmol^{-1}). Thus the plot of $1/\eta$ against $1/C_{eq}$ should be linear with a slope of $1/(\eta_{max}K_L)$ and an intercept of $1/\eta_{max}$ on the $1/\eta$ axis.
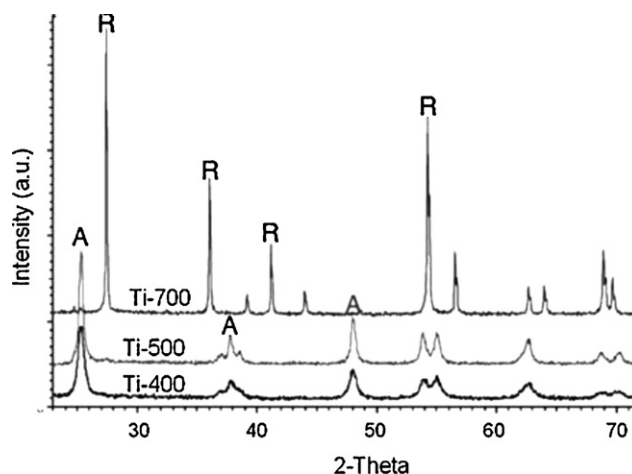

Fig. 1. XRD patterns of Ti-400, Ti-500 and Ti-700 samples. Diffraction peaks corresponding to anatase and rutile structures are respectively indexed by the letters A and R.
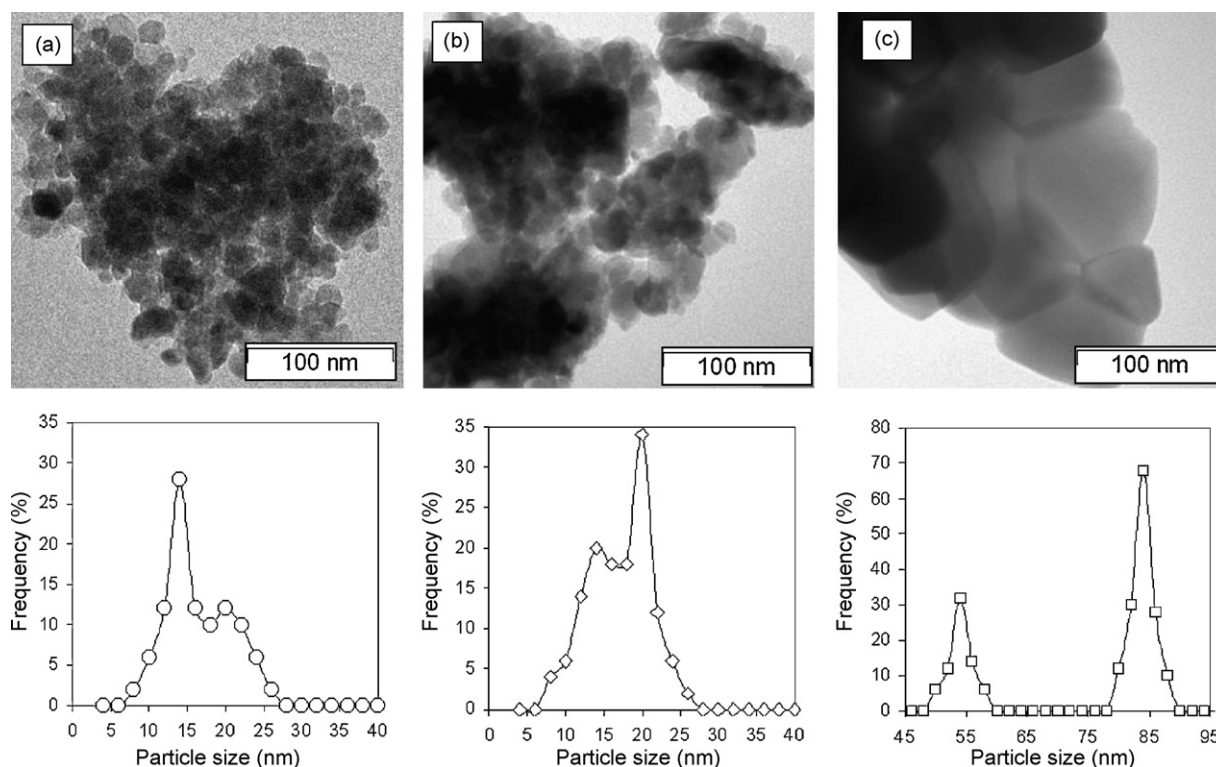
Fig. 2. TEM images and particle size distribution of: (a) Ti-400, (b) Ti-500 and (c) Ti-700.

2.5. Photocatalytic activity

The photocatalytic degradation of dyes (methylene blue, MB, and crystal violet, CV) under visible light irradiation ($\lambda \geq 400$ nm), was carried out using a 50 mL batch reactor with external lamp (Silvana, HI-spot ES 50W/WFL50 °C). The photocatalytic degradation of dyes under UV irradiation was carried out under a high-pressure mercury lamp (150 W, 220 V, $\lambda \geq 360$ nm). A circulating water jacket was used to cool the batch reactor and the temperature was kept around 25 °C. In a typical experiment, TiO_2 powder was added to an aqueous solution (20 μmol L^{-1}) of dye to reach a concentration of 1 g L^{-1}. In all cases, the mixture was kept in the dark to ensure that the adsorption–desorption equilibrium was reached before illumination. After a given irradiation time, samples were taken out from reactor, then the catalyst was removed by centrifugation and the remaining dye concentration in the solution was measured by light absorption of clear solution at 664 nm for MB and 546 nm for CV ($C_{25}H_{30}ClN_3$). Additionally, to check the stability of the Ti-700 sample, at the end of each photoreactivity experiment, the resulting suspension was centrifugalized, the solution was removed, and the separated catalyst was washed with demonized water and reused for the further photocatalytic experiment. This process was repeated four times.

3. Results

3.1. Catalyst characterization

Fig. 1 illustrates the XRD patterns of samples calcined at 400, 500 and 700 °C. Calcination at 400 and 500 °C (Ti-400, Ti-500) leads to well defined diffraction peaks corresponding to the anatase phase, whereas, at 700 °C a total anatase-to-rutile transition phase is observed. In addition, as the calcination temperature rises, XRD reflections become narrower, indicating changes in crystallite size. Fig. 2 shows the TEM images and particle size distributions of the TiO_2-xerogels after calcination

and H_2-HTR treatment. The crystallite sizes (L, nm) are showed in Table 1. A higher temperature causes a strong rapid increase in L from ~16 to ~85 nm, for Ti-400 and Ti-700, respectively.

Fig. 3 shows nitrogen adsorption–desorption isotherms. The values of the specific surface area, S_{BET}, and the pore volume, V_p, are displayed in Table 1. While the Ti-NC sample develops an

Table 1
Characteristics of the catalysts.

Sample	Crystalline phase (TiO_2)	L (nm)	S_{BET} (m^2 g^{-1})	V_p (cm^3 g^{-1})	E_g (eV)
Ti-NC	Amorphous	–[a]	260	0.15	3.61
Ti-400	Anatase	16	20	0.06	3.16
Ti-500	Anatase	18	5	0.04	3.15
Ti-700	Rutile	55, 85	2	0.03	3.04

L: crystallite size; S_{BET}: specific surface area; V_p: total pore volume; E_g: band-gap energy.
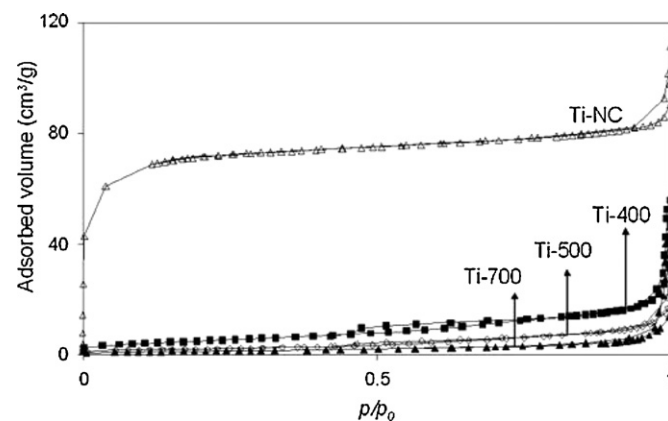[a] Not measured.

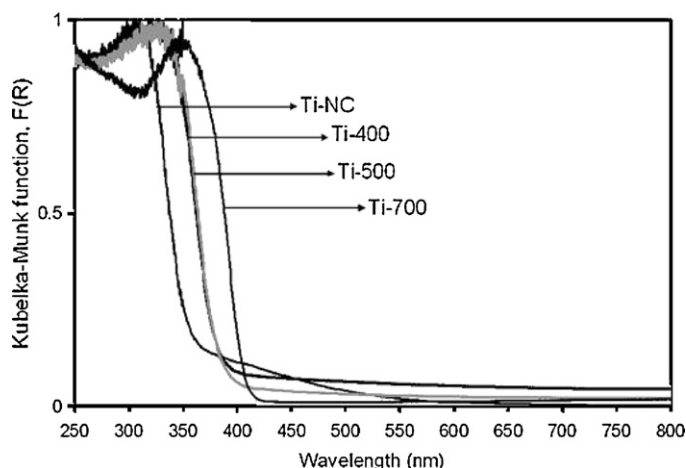**Fig. 3.** Nitrogen adsorption–desorption isotherms of Ti-NC, Ti-400, Ti-500 and Ti-700 samples.

Fig. 4. DR UV/Vis spectra of Ti-NC, Ti-400, Ti-500 and Ti-700 samples.

Table 2
Adsorption of MB: parameters of Langmuir isotherms.

Sample	η_{max} ($\mu mol\,g^{-1}$)	Γ_{max} ($\mu mol\,m^{-2}$)	K_L ($\times 10^5\,L\,mol^{-1}$)	S_{MB} ($m^2\,g^{-1}$)	S_{MB}/S_{BET}
Ti-NC	3.7	0.1	7.2	26.9	0.10
Ti-400	0.2	0.1	11.3	1.6	0.08
Ti-500	0.2	0.4	9.2	1.5	0.29
Ti-700	0.1	0.9	8.8	1.4	0.69

η_{max}: amount of adsorbate (MB) at monolayer coverage; Γ_{max}: maximal amount of adsorbate (MB) at monolayer coverage by surface area unit; K_L Langmuir equilibrium constant of adsorption; S_{MB}: surface area covered by MB.

important porous texture; its calcination at high temperature induces the collapse of this porous texture. In particular S_{BET}, which is $260\ m^2\,g^{-1}$ for Ti-NC, decreases 20, 5 and $2\ m^2\,g^{-1}$ for Ti-400, Ti-500 and Ti-700 samples, respectively.

DR-UV/Vis spectra of all samples are shown in Fig. 4. A maximal absorption band (λ_{max}) is observed in the 310–360 nm region. This band corresponds to the $O^{2-}(2p) \rightarrow Ti^{4+}(3d)$ charge transfer process in TiO_2 (anatase: $\lambda_{max} = 325\ nm$; rutile: $\lambda_{max} = 350\ nm$). The Ti-NC sample displays a band-gap value of 3.61 eV, whereas Ti-400 and Ti-500 show a band-gap value of 3.16 and 3.15 eV, respectively (Table 1). As the calcination temperature increases up to 700 °C and the rutile phase appears the band-gap decreases to around 3.04 eV.

The IR absorbance spectra of all TiO_2 xerogels are compared in Fig. 5a within the $700–4000\ cm^{-1}$ range. All samples show the fundamental vibrations of TiO_2 [41–44]. These vibrations appear as very intense absorption bands at around $500\ cm^{-1}$, ascribed to Ti–O and Ti–O–Ti bonds. The vibration modes of the $Ti^{4+}O–H$ and adsorbed H_2O are found at around 3300 and $1630\ cm^{-1}$ respectively on the spectrum of Ti-NC but have disappeared after calcination and H_2-HTR treatments. After those thermal treatments, bands next to $2900\ cm^{-1}$ and in the $900–1500\ cm^{-1}$ region both associated with organic residues have also disappeared. Additionally, together with the increase

in the calcination temperature (400, 500, 700 °C), a dramatic increase in absorbance in the entire IR spectrum is observed. This increase is also accompanied by the appearance of multiple peaks in the OH stretching region (next to $3600\ cm^{-1}$). Fig. 5b shows the evolution of the IR background absorbance (as measured at $2000\ cm^{-1}$) as a function of calcination temperature.

3.2. Adsorption isotherms of methylene blue (MB)

Table 2 summarizes the parameters of Langmuir isotherms used to describe the adsorption of MB on all samples (Fig. 6a and b). The maximal amount of adsorbate at monolayer coverage by surface area unit, Γ_{max}, was obtained by dividing η_{max} by the specific surface area, S_{BET}, of the sample (Table 2) [45]. The specific surface area covered by methylene blue, S_{MB} ($m^2\,g^{-1}$), was obtained by multiplying η_{max} ($mol\,g^{-1}$) by the effective area of MB ($7.2 \times 10^5\ m^2\,mol^{-1}$), assuming that the MB molecule lies flat on the TiO_2 surface [46,47]. Fig. 7 shows the evolution of Γ_{max} values as a function of calcination temperature.

3.3. Photocatalytic activity

The activities of the catalysts were evaluated in the photoconversion of MB and CV at room temperature, under UV and visible light irradiation. The control tests confirm that MB and CV are not degraded in the dark in the presence of catalyst and only the CV is slightly degraded under UV light irradiation in the absence of catalyst. It is referred to as black, Fig. 9a and b. The evolution of the dye concentration as a function of time is shown in Figs. 8a, 9a, 10a and 11a. Analyses
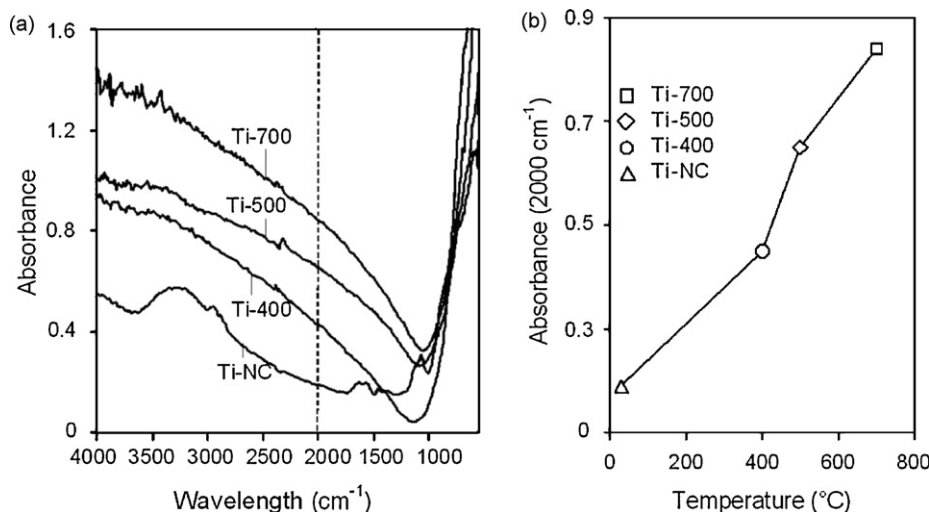

Fig. 5. (a) IR absorbance spectra of Ti-NC, Ti-400, Ti-500 and Ti-700 samples; (b) evolution of IR background absorbance (as measured at $2000\ cm^{-1}$) as a function of calcination temperature.
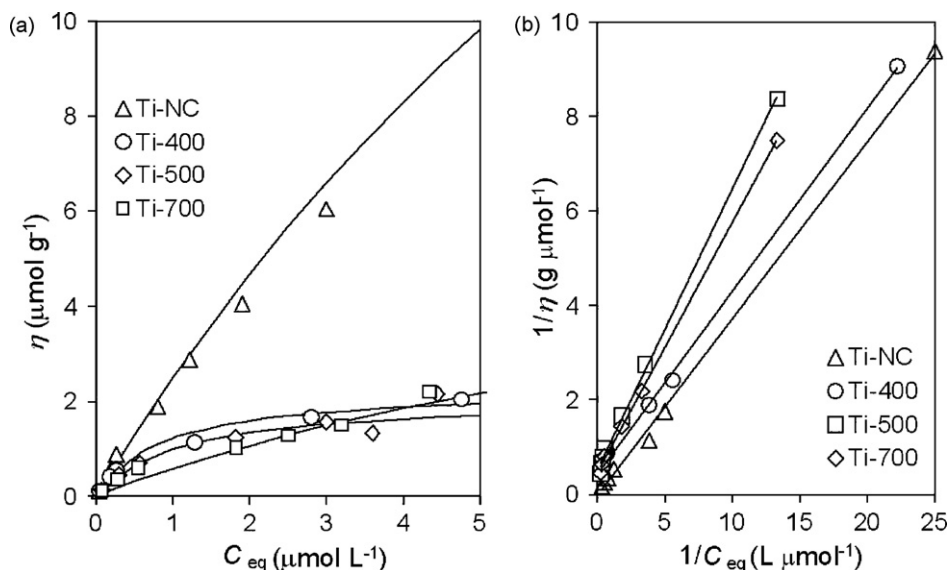
Fig. 6. (a) Adsorption isotherms of MB on all samples in aqueous solution; (b) corresponding linear Langmuir adsorption isotherms of MB.

of these curves were carried out with the Langmuir–Hinshelwood (L–H) kinetic model [32,48–50]:

$$r_S = \frac{kKC}{1 + KC} \tag{2}$$

where r_S is the specific degradation reaction rate the dye (mol L^{-1} s^{-1}), C the concentration of the dye (mol L^{-1}), k the reaction rate constant (s^{-1}) and K is the dye adsorption constant. When the concentration (C) is small enough, Eq. (2) can be simplified in an apparent first-order equation:

$$r_S = kKC = K_{app}C\left(= -\frac{dC}{dt}\right) \tag{3}$$

After integration, Eq. (4) is obtained.

$$-\ln\left(\frac{C}{C_0}\right) = K_{app}t \tag{4}$$

where C_0 is the initial concentration (mol L^{-1}) and t the illumination time (s). In all cases, an acceptable linearity was

Fig. 7. Evolution of Γ_{max} as a function of calcination temperature.

obtained by applying equation (4) (Figs. 8b, 9b, 10b and 11b), and values of the apparent first-order constant, K_{app}, are reported in Table 3. For each catalyst, the initial rate of decomposition of methylene blue (r_0^{MB}) and crystal violet (r_0^{CV}) were calculated by multiplying K_{app} by the initial dye concentration ($C_0 = 20$ μmol L^{-1}).

$$r_0 = K_{app}C_0 \tag{5}$$

For non-porous catalysts such as Ti-700 and P25, another approach to determine the efficiency of photocatalysts r_A (mol m^{-2} s^{-1}) can be adopted by referring the rate of dye photoconversion to the external surface area of irradiated catalyst [52]:

$$r_A = \frac{V}{A}r_0 \tag{6}$$

where A is the external area of irradiated catalyst (m^2 g^{-1}) and V is the total reaction volume (L).

3.3.1. Photoactivity under UV light irradiation

The evolution of MB concentration under UV light irradiation as a function of time is shown in Fig. 8a. A strong increase in the initial rate of MB photocatalytic degradation, r_0^{MB}, is observed after calcination and H$_2$-HTR treatment (Table 3). In addition, the calcined samples (Ti-400, Ti-500, Ti-700) displayed similar r_0^{MB} values, to around 1.2×10^{-9} mol L^{-1} s^{-1}. However, in contrast with several studies [24–28], the rutile-TiO$_2$ (sample Ti-700) does not show a significant decrease in photocatalytic activity in spite of its lower specific surface area ($S_{BET} = 2$ m^2 g^{-1}).

Similar results are observed in the photo-degradation of crystal violet (CV). The behaviour of CV concentration as a function of time under UV irradiation is shown in Fig. 9a. The samples calcined and H$_2$-HTR treated (Ti-400, Ti-500 and Ti-700) showed an apparent rate of photoconversion between 11.7 and 17.3×10^{-9} mol L^{-1} s^{-1}, whereas the non-calcined sample displayed it at 0.53×10^{-9} mol L^{-1} s^{-1} (Table 3). In comparison with MB, the CV was degraded in its totality after 40 min of UV light irradiation.

3.3.2. Photoactivity under visible light irradiation

The changes in the concentration of MB recorded during visible light irradiation at specific time intervals are shown in
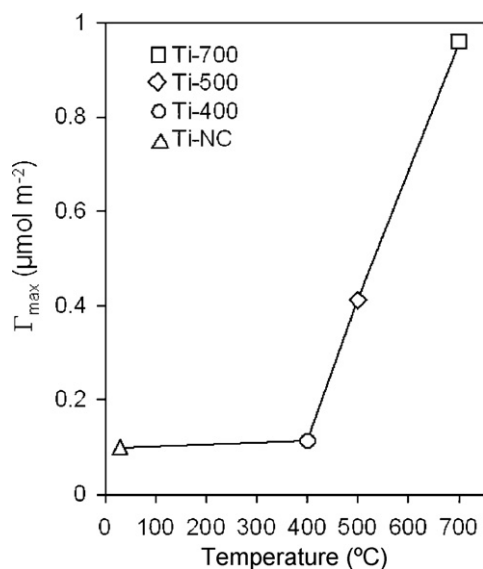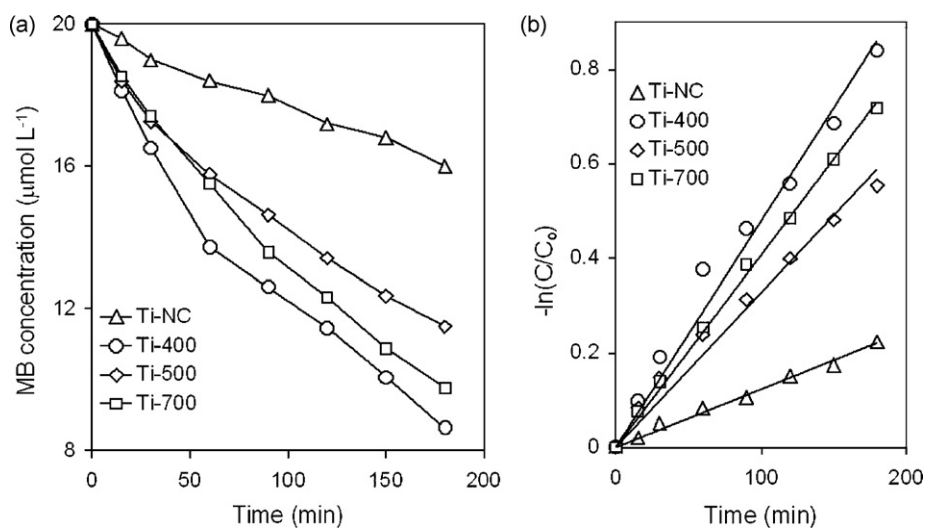
Fig. 8. (a) Photo-degradation of MB under UV light irradiation as a function of reaction time; (b) first-order relationship $-\ln(C/C_0) = K_{app}t$.
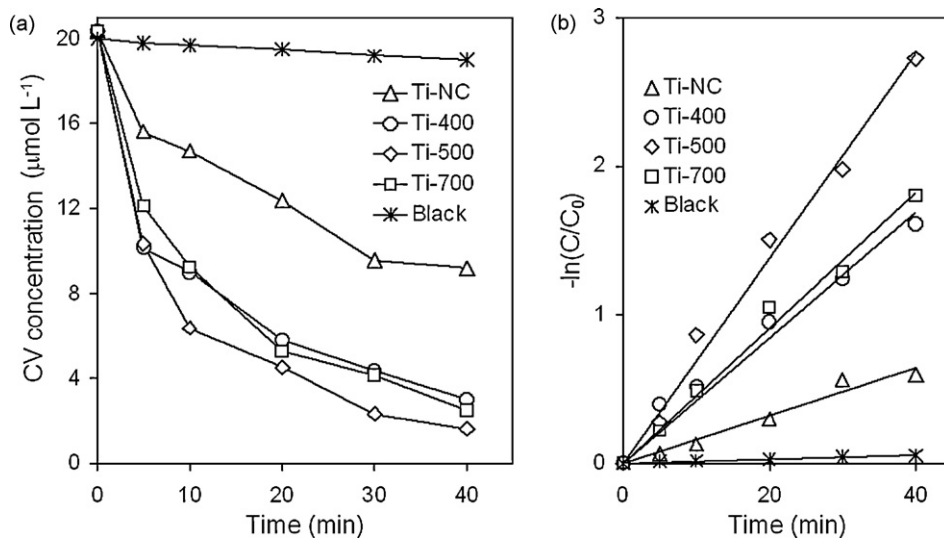

Fig. 9. (a) Photo-degradation of CV under UV light irradiation as a function of reaction time; (b) first-order relationship $-\ln(C/C_0) = K_{app}t$.
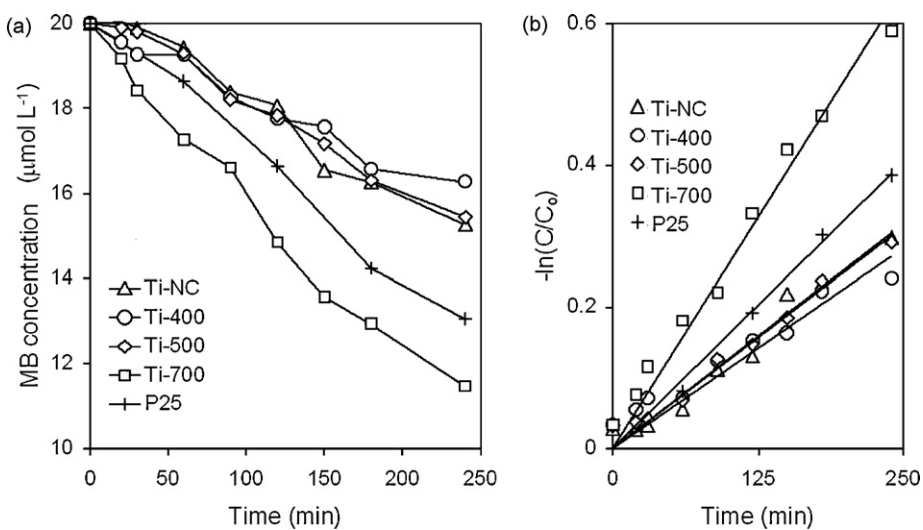

Fig. 10. (a) Photo-degradation of MB under visible light irradiation as a function of reaction time; (b) first-order relationship $-\ln(C/C_0) = K_{app}t$.
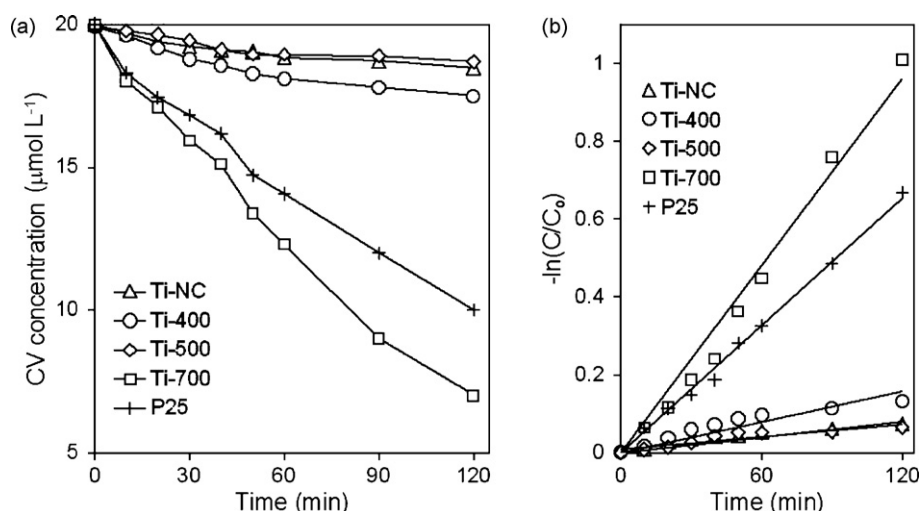
Fig. 11. (a) Photo-degradation of CV under visible light irradiation as a function of reaction time; (b) first-order relationship $-\ln(C/C_0) = K_{app}t$.

Table 3
Kinetic parameters of the photo-degradation of MB and CV under UV and visible light irradiation.

Sample	Methylene blue (MB)				Crystal violet (CV)			
	UV light		Visible light		UV light		Visible light	
	K_{app}^{MB} $(\times 10^5\,s^{-1})$	r_0^{MB} $(\times 10^9\,mol\,L^{-1}\,s^{-1})$	K_{app}^{MB} $(\times 10^5\,s^{-1})$	r_0^{MB} $(\times 10^9\,mol\,L^{-1}\,s^{-1})$	K_{app}^{CV} $(\times 10^5\,s^{-1})$	r_0^{CV} $(\times 10^9\,mol\,L^{-1}\,s^{-1})$	K_{app}^{CV} $(\times 10^5\,s^{-1})$	r_0^{CV} $(\times 10^9\,mol\,L^{-1}\,s^{-1})$
Ti-NC	2.0	0.4	2.0	0.4	2.6	0.53	0.8	0.1
Ti-400	7.3	1.4	1.5	0.3	58.3	11.7	1.8	0.3
Ti-500	5.0	1.0	1.8	0.3	86.3	17.3	0.8	0.1
Ti-700	6.5	1.3	3.8	0.7	71.6	14.3	14.5	2.9
P25	–	–	2.8	0.5	–	–	9.1	1.8

K_{app}: apparent first-order constant; r_0: initial reaction rates of dye.

Fig. 10a. Commercially available TiO$_2$ (Degussa P25) was used as a reference photocatalyst. In contrast with the behaviour observed under UV light irradiation, under visible light irradiation no significant differences were found in the photo-activity between the non-calcined sample (Ti-CN) and the samples calcined at 400 and 500 °C (Ti-400, Ti-500), which show values of about 0.35×10^{-9} mol L^{-1} s^{-1} for the photoconversion rate, r_0^{MB} (Table 3). Ti-700 displays a higher r_0^{MB} value of 0.7×10^{-9} mol L^{-1} s^{-1}.

Fig. 11a shows the photocatalytic activity of all TiO$_2$ xerogels in the degradation of CV in the presence of visible light. Again, the rutile-TiO$_2$ (Ti-700) displays a notable increase in the photo-catalytic degradation of CV, compared with Ti-NC, Ti-400 and Ti-500. After 120 min of visible light irradiation about 80% of CV was degraded by Ti-700, whereas only a 10% was degraded by the TiO$_2$ xerogels calcined below 600 °C.

Finally, in comparison with the commercial TiO$_2$ (Degussa P25) with a $S_{BET} \cong 55$ m^2/g and a crystalline distribution of 80%-anatase, 20%-rutile, the rutile-TiO$_2$ (Ti-700) synthesized in this study by the sol–gel process shows an efficiency by external surface area, r_A, up to 40 times higher in the photoconversion of MB and CV under visible light irradiation (Fig. 12a). In addition, Fig. 12b displays how the Ti-700 sample can be recycled four times in the MB and CV photo-degradation.

4. Discussion

The changes observed in the physicochemical properties of TiO$_2$ xerogels after calcination at 400, 500, 700 °C and high temperature reduction at 400 °C under hydrogen flow (calcination/H$_2$-HTR treatment) are totally in accordance with results found in the literature [24,28,53–56]. An increase in the crystalline level of

anatase-TiO$_2$ phase was observed when a Ti-NC sample was calcined a 400 and 500 °C (Ti-400, Ti-500, Fig. 1), whereas at 700 °C a total anatase-to-rutile phase transformation (Ti-700) was determined. These changes were accompanied by: (i) the growth of crystalline size, L, from 16 to 85 nm (Table 1), (ii) a strong decrease in the specific surface area, S_{BET}, from 260 to about of 2 m^2 g^{-1} (Table 1), and (iii) a decrease in the band-gap energy, E_g, from 3.61 to 3.04 eV when the rutile phase appeared (Table 1).

Applying thermal treatment to titanium dioxide can lead to structural changes, which are characteristic of diffusion processes associated with the increased mobility of lattice defects and with the changes in oxygen vacancies in TiO$_2$-lattice (such as Ti^{3+}). The production of electronic defects in an n-type semiconductor such as TiO$_2$, via thermal reduction leads to an increase in the IR background absorbance of TiO$_2$ within a range from 3000 to 1000 cm^{-1} [57–61]. In fact, this effect can be observed in Fig. 5: the calcination and H$_2$-HTR treatment cause an increase in the IR background absorbance in the TiO$_2$ xerogels. Specifically, Fig. 5b shows that this absorbance, measured at 2000 cm^{-1}, is augmented together with the increase in calcination temperature.

It has been demonstrated that the surface defect sites (oxygen vacancies) act as electron donors and are the specific sites for H$_2$ adsorption [4]. The IR absorption increase observed in Fig. 5 might be interpreted as absorption by electronic defects on the microcrystalline level, considering that these electronic changes in the solid structure might be a consequence of hydrogen atom presence into TiO$_2$. Therefore, the order of increase in the IR absorbance can be correlated with the increase in the surface defect sites in support of TiO$_2$ [62]. So, the calcination at 700 °C (Ti-700) and the H$_2$-HTR treatment lead to a greater reduction in the degree of support. Additionally, in the IR absorbance spectra of Ti-700 the appearance of signals in the stretching band area of TiO-H,
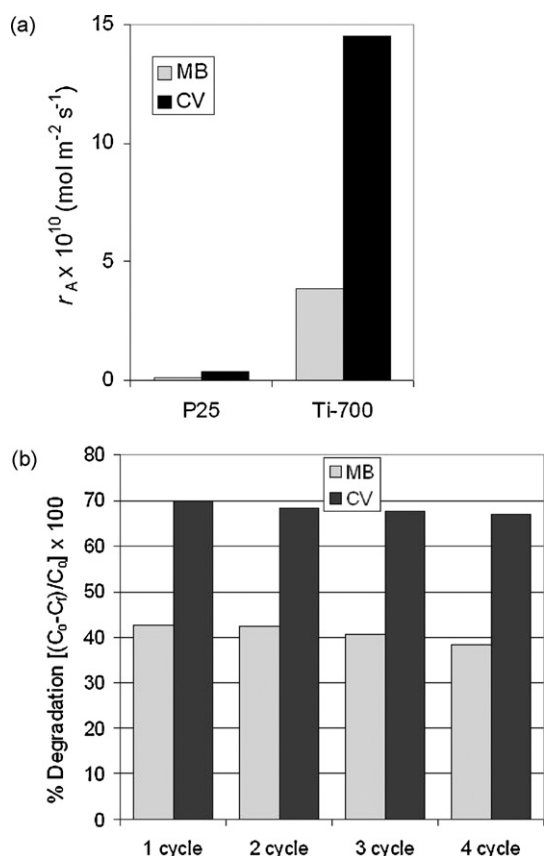
Fig. 12. (a) Comparison between the photocatalytic efficiencies of Ti-700 and P25 in the degradation of MB and of CV; (b) Ti-700 photo-catalyst reusability in the MB and CV degradation under visible irradiation.

next to 3660 cm^{-1}, is presumably evidence of a higher presence of hydrogen atoms in the bulk of rutile-TiO$_2$.

The changes in the reduction degree of support affect the adsorption process through the presence of the TiO$_2$ surface defect sites. The effect of calcination and H$_2$-HTR treatment in the MB adsorption capacity of non-calcined TiO$_2$ (Ti-NC) is studied in Fig. 6a. All adsorption isotherms show L shape curves according to the classification of Giles et al. [63,64]. The L shape of the adsorption isotherms means that there is no strong competition between the solvent and the adsorbate to occupy the adsorbent surface sites. In this case, the longitudinal axes of the adsorbed molecules are parallel to the adsorbent surface (molecules adsorbed flat on the surface) [65]. The isotherms fit well with the Langmuirian type, implying a monolayer adsorption model (Eq. (1), Fig. 6b) [48,66–68]. Additionally, the ratios of specific surface area covered by MB are less than 1: S_{MB}/S_{BET} varies from 0.1 to 0.7 (Table 2), and this value should indicate a dye monolayer coverage without aggregation of MB. After calcination and H$_2$-HTR treatment of Ti-NC, results show that the maximal amount of MB at monolayer coverage by surface area unity (Γ_{max}) is strongly increased (up to 9 times higher for Ti-700) together with the increase in calcination temperature, even if the S_{BET} strongly decreases (Fig. 7). This means that the density of surface active sites for MB adsorption by surface area unit is increased, possibly as a consequence of the increase in the surface defect sites produced by the H$_2$ reduction of TiO$_2$ surface.

In the photoconversion of MB and CV under UV light irradiation (Figs. 8a and 9a), no remarkable differences between the Ti-400, Ti-500 and Ti-700 are found. According to several authors [22–28], the anatase-to-rutile phase transformation of TiO$_2$ greatly reduces the specific surface area of the particles, which may result in the

decrease in the photocatalytic activity of rutile. In contrast, in this study, the photocatalytic activity of the sample calcined at 700 °C is conserved even if a total anatase-to-rutile phase transformation is observed and its specific surface area is reduced to 2 m^2 g^{-1}. In agreement with the analysis proposed by Konstantinou et al. [50], the rate of photoconversion of dye with UV-irradiated TiO$_2$ follows the Langmuir–Hinshelwood (L–H) law for four possible situations: (i) the reaction takes place between two adsorbed substances, (ii) the reaction occurs between a radical (such as O$_2^{\bullet-}$, HO$_2^{\bullet-}$, OH$^{\bullet}$) in solution and an adsorbed dye molecule, (iii) the reaction takes place between a radical linked to the surface and a dye molecule in solution, and (iv) the reaction occurs with the both species being in solution. In all cases, the expression for the rate equation is similar to that derived from the L–H model, although it is not possible to find out whether the process takes place on the surface, in the solution or at the interface [51]. It is likely that adsorption of the dye plays an important role in the photocatalytic degradation rates. The improvement in the MB adsorption ability shown by Ti-700 (Γ_{max} value, Fig. 7) together with its higher reduction degree (key in the O$_2$ adsorption and subsequent production of radicals) may explain its photo-degradation capacity in comparison with samples calcined at 400 and 500 °C.

The MB and CV photoconversions under visible light irradiation show the following of a different pathway than under UV light irradiation. In comparison with the photoconversion under UV light (Figs. 8a and 9a), in the photoconversion under visible irradiation, the rutile-TiO$_2$ (Ti-700) is the catalyst with the highest capacity for the photo-degradation of MB and CV (Figs. 10a and 11a). The significantly enhanced in r_0^{MB} and r_0^{CV} displayed by Ti-700 under visible light can be explained through the following mechanism: (i) unlike in the Ti-NC, Ti-400 and Ti-500 samples, the rutile-TiO$_2$ (Ti-700) can be excited by visible irradiation ($\lambda \geq 400$ nm, $E_g \cong 3.04$ eV), (ii) more dye molecules are adsorbed (by surface area unity) into Ti-700 (Γ_{max}), enhancing the electron transfer from the photo-excited dye to the conduction band of TiO$_2$ and subsequently increasing the electron transfer to the absorbed O$_2$, and (iii) the highest reduction degree observed in Ti-700 may favour the O$_2$ adsorption and subsequent production of radicals.

Finally, only the commercial TiO$_2$ (P25) displays a photocatalytic ability comparable with Ti-700 under visible irradiation. However, the photoconversion efficiency referred to the irradiated surface area, r_A, shown by Ti-700 is up to 40 times higher than for P25. Additionally, Ti-700 sample showed very good stability under irradiation conditions and can be recycled four times without significant loss of activity.

5. Conclusion

A series of H$_2$-reduced TiO$_2$ xerogels of low specific surface area were obtained by calcination (at 400, 500 and 700 °C) and high temperature reduction at 400 °C under hydrogen flow (H$_2$-HTR). Predictable changes in their physicochemical characteristics were determined after H$_2$-HTR and calcination at 700 °C; (i) total anatase-to-rutile phase transformation, (ii) growth of crystalline size, (iii) decrease in the specific surface area, and (iv) diminution in the band-gap energy from 3.61 to 3.02 eV for Ti-700. However, the greater degree of reduction shown by the rutile-TiO$_2$ lattice (Ti-700) led to unpredictable photocatalytic properties in the dye conversion under UV and visible light irradiation. The loss in the specific surface area observed was compensated by the increase in the surface active sites for adsorption of MB and the augment in its affinity by the MB. These effects presumably allowed the improvement in the performance of rutile-TiO$_2$, reaching a photocatalytic ability comparable to, or better than, the analogous anatase-TiO$_2$ xerogels (Ti-400, Ti-500), under UV light irradiation. By contrast, under visible light irradiation only rutile-TiO$_2$ xerogel

(Ti-700) showed a remarkable photo-efficiency, possibly due to a combined effect between the potential photo-sensitivity of its band gap and the electron transfer from photo-excited dye to the surface of Ti-700. Additionally, the photoconversion rate referred to the surface area unity displayed by rutile-TiO_2 was up to 40 times higher than commercially available P25.

Acknowledgements

References

[1] M.R. Hoffman, S.C. Martin, W. Choi, D.W. Bahnemann, Chem. Rev. 95 (1995) 69.
[2] A. Hogelt, M. Grätzel, Chem. Rev. 95 (1995) 49.
[3] M.A. Fox, M.T. Dulay, Chem. Rev. 93 (1993) 341.
[4] A.L. Linsebigler, G. Lu, J.T. Yates Jr., Chem. Rev. 95 (1995) 735.
[5] C. Kormann, D.W. Bahnemann, M.R. Hoffman, J. Phys. Chem. 92 (1998) 5196.
[6] W. Choi, A. Termin, M.R. Hoffman, J. Phys. Chem. 98 (1994) 13669.
[7] G. Granados, C.A. Páez, F. Martínez, E.A. Páez-Mozo, Catal. Today 107–108 (2005) 589.
[8] T. Wu, G. Liu, J. Zhao, H. Hidaka, N. Serpone, J. Phys. Chem. B 102 (1998) 5845.
[9] A. Fujishima, T.N. Rao, D.A. Tryk, J. Photochem. Photobiol. C: Photochem. Rev. 1 (2000) 1.
[10] H.M. Sung-Suh, J.R. Choi, H.J. Hah, S.M. Koo, Y.C. Bae, Photochem. Photobiol. A: Chem. 163 (2004) 37.
[11] A. Wold, Chem. Mater. 5 (1993) 280.
[12] A. Sclafani, J.-M. Hermann, Photochem. Photobiol. A: Chem. 113 (1998) 181.
[13] B. Braconnier, C.A. Páez, S. Lambert, C. Alié, C. Henrist, D. Poelman, J.-P. Pirard, R. Cloots, B. Heinrichs, Micropor. Mesopor. Mater. 122 (2009) 247.
[14] F. Galindo, R. Gómez, M. Aguilar, J. Mol. Catal. A: Chem. 281 (2008) 119.
[15] C. Anderson, A.J. Bard, J. Phys. Chem. B 101 (1997) 2611.
[16] D. Shukin, S. Poznyak, A. Kulak, P. Pichat, J. Photochem. Photobiol. A: Chem. 162 (2004) 423.
[17] J. Aguado, R. Van Grieken, M.J. López-Muñoz, J. Maragan, Appl. Catal. A: Gen. 312 (2006) 202.
[18] K. Nagaveni, M.S. Hegde, N. Ravishankar, G.N. Subbanna, G. Madras, Langmuir 20 (2004) 2900.
[19] S.U. Khan, M. Al-Shahry, W.B. Ingler, Science 297 (2002) 2243.
[20] R. Asahi, T. Morikawa, T. Ohwaki, K. Aoki, Y. Taya, Chem. Phys. 399 (2007) 57.
[21] R. Zhang, L. Gao, Q. Zhang, Chemosphere 54 (2004) 405.
[22] J.C. Yu, J. Yu, L. Zhang, W. Ho, Photochem. Photobiol. A: Chem. 148 (2002) 263.
[23] R. Arroyo, G. Córdoba, J. Padilla, V.H. Lara, Mater. Lett. 54 (2002) 397.
[24] P. Górska, A. Zaleska, E. Kowalska, T. Klimczu, J.M. Sobczak, E. Skwarek, W. Janusz, J. Hupka, Appl. Catal. B: Environ. 84 (2008) 440.
[25] Q. Xiao, J.J. Zhang, C. Xiao, Z. Si, X. Tan, Solar Energy 82 (2008) 706.
[26] C. Su, B.-Y. Hong, C. Tseng, Catal. Today 96 (2004) 119.
[27] G. Li, S. Ciston, Z. Saponjic, L. Chen, N.M. Dimitrijevic, T. Rajh, K.A. Gray, J. Catal. 253 (2008) 105.
[28] H. Zhang, J.F. Banfield, J. Phys. Chem. B 104 (2000) 3481.
[29] K.J. Kim, K. Benksten, J. Van de Lagemaat, A.T. Frank, Chem. Mater. 14 (2002) 1042.
[30] H. Byun, R. Vittal, D.Y. Kim, K.J. Kim, Langmuir 20 (2004) 6853.
[31] S. Zhang, C.-Y. Liu, Y. Liu, Z.-Y. Zhang, L.-Y. Mao, Mater. Lett. 63 (2009) 127.
[32] M.M. Mohamed, M.M. Al-Esaimi, J. Mol. Catal. A: Chem. 255 (2006) 53.
[33] Y. Yang, C. Guo, C. Hu, Y. Wang, E. Wang, Appl. Catal. A: Gen. 273 (2004) 201.
[34] W. Göpel, G. Rocker, K. Feierabend, Phys. Rev. B 28 (1983) 3427.
[35] R.L. Kurtz, K. Stockauer, T.E. Madey, E. Roman, J.L. De, Segovia, Surf. Sci. 218 (1989) 178.
[36] H. Idriss, K.S. Kim, M.A. Barteau, Surf. Sci. 262 (1992) 113.
[37] H. Liu, H.T. Ma, X.Z. Li, W.Z. Li, M. Wu, X.H. Bao, Chemosphere 50 (2003) 39.
[38] A.J. Lecloux, in: J.R. Anderson, M. Boudart (Eds.), Catalysis: Science and Technology, Springer, Berlin, 1981, p. 171.
[39] P. Kubelka, F. Munk, Zeit. Für Tekn. Physik 12 (1931) 593.
[40] C. Colon, M. Maicu, M.C. Hidalgo, J.A. Navio, Appl. Catal. B: Environ. 67 (2006) 41.
[41] J. Araña, A. Peña Alonso, J.M. Doña Rodriguez, G. Colón, J.A. Navio, J. Pérez Peña, Appl. Catal. B: Environ. 89 (2009) 204.
[42] K. Chhor, J.F. Bocquet, C. Pommier, Mater. Chem. Phys. 32 (1992) 249.
[43] T. Bezrodna, G. Puchkovska, V. Shymanovska, J. Bara, H. Ratajczak, J. Mol. Struct. 700 (2004) 175.
[44] A. Larbot, I. Laaziz, J. Marignan, J.F. Quinson, J. Non-Cryst. Solids 147–148 (1992) 157.
[45] J. Moser, S. Punchihewa, P.P. Infelta, M. Grätzel, Langmuir 7 (1991) 3012.
[46] A. Abdel-Nasser, E. Hendawg, Carbon 41 (2003) 713.
[47] A.P. D'Silva, Carbon 36 (1998) 1317.
[48] A. Houas, H. Lachhed, M. Ksibi, E. Elaloui, C. Goillard, J.M. Hermann, Appl. Catal. B: Environ. 31 (2001) 145.
[49] C. Galindo, P. Jacques, A. Kalt, Photochem. Photobiol. A: Chem. 130 (2000) 35.
[50] I.K. Konstantinou, T.A. Albanis, Appl. Catal. B: Environ. 49 (2004) 1.
[51] A. Bianco-Prevot, C. Baiocchi, M.C. Brussino, E. Pramauro, P. Savarino, V. Augugliaro, G. Marci, L. Palmisaro, Environ. Sci. Technol. 35 (2001) 971.
[52] H. de Lasa, B. Serrano, M. Salaices (Eds.), Photocatalytic Reaction Engineering, Springer, USA, 2005, pp. 1–15.
[53] J.F. Porter, Y. Li, C.K. Cahn, J. Mater. Sci. 34 (1999) 1523.
[54] K.M. Reddy, C.V.G. Reddy, S.V. Manorama, J. Solid State Chem. 158 (2001) 180.
[55] H.F. Yu, J. Phys. Chem. Solids 68 (2007) 600.
[56] A. Pottier, C. Chaneac, E. Tronc, K. Mazerolles, J.P. Jolivet, J. Mater. Chem. 11 (2001) 1116.
[57] P.A. Panayotov, J.T. Yates, Chem. Phys. Lett. 410 (2005) 11.
[58] P.A. Panayotov, J.T. Yates, Chem. Phys. Lett. 399 (2004) 300.
[59] S.H. Szczepankiewicz, J.A. Moss, M.R. Hoffmann, J. Phys. Chem. B 106 (2002) 2922.
[60] S.H. Szczepankiewicz, A. Colussi, M.R. Hoffmann, J. Phys. Chem. B 104 (2000) 9842.
[61] A. Yamaka, T. Ishibashi, H. Onishi, J. Phys. Chem. B 105 (2001) 7258.
[62] E.V. Benvenutti, L. Franken, C.C. Moro, Langmuir 15 (1999) 8140.
[63] C.H. Giles, T.H. MacEwan, S.N. Nakhwa, D. Smith, J. Chem. Soc. 10 (1960) 3973.
[64] C.H. Giles, A.P. Da Silva, I.A. Easton, J. Colloid Interf. Sci. 47 (1974) 766.
[65] O. Hamdaouia, E. Naffrechoux, J. Hazard. Mater. 147 (2007) 381.
[66] Y. Xu, C.H. Langford, Langmuir 17 (2001) 897.
[67] T. Sauer, G.C. Neto, H.J. Jose, R.F. Moreira, J. Photochem. Photobiol. A: Chem. 149 (2002) 147.
[68] H. Lachheb, E. Puzenat, A. Houas, M. Ksibi, E. Elaoui, G. Guillard, J.M. Hermann, Appl. Catal. B: Environ. 39 (2002) 75.